

STELLAR X-RAY EMISSION*

PHILIP C. FISHER AND ARTHUR J. MEYEROTT

Lockheed Missiles and Space Company, Research Laboratories, Palo Alto, California

Received January 21, 1963; revised August 7, 1963

ABSTRACT

Measurements of night-sky regions emitting photons having energies between 1 and 20 keV are described. Isophote plots are given for a portion of the sky near 5 hours of right ascension for photons in three non-contiguous energy intervals. The plots were derived from data obtained from several different gas-proportional counters carried aboard each of two sounding rockets. Locations of at least six regions, emitting photons in at least two of the three different energy intervals, are given. Absolute luminosities for 2–8-Å photons are presented for the nearest of the stellar objects tentatively associated with these regions.

I. INTRODUCTION

Some results of an experiment which appears to have successfully identified stellar sources of soft X-rays are presented here. Soft X-rays are arbitrarily defined in this paper as photons having energies between 0.2 and 20 keV, although emphasis will be on data for 1 to 20 keV photons.

Speculation about the necessary physical conditions for X-ray emission and calculation of features of the spectra emitted from celestial objects have been carried on over a number of years (Elwert 1954, 1961; de Jaeger 1959; Olbert 1960; Felten and Morrison 1963). Both radio and stellar sources have been considered, the spectra from these emitters being characterized, respectively, as a continuum due to synchrotron radiation and a continuum (of some admixture of Bremsstrahlung, black-body, and synchrotron radiation) with superimposed emission lines. A calculation for the X-ray flux from intergalactic matter has also been made (Hoyle 1963).

In early 1960, development of suitable experimental techniques was begun in order to attempt a scan of the night sky. The ultimate purpose of the investigation was to obtain information about the physical properties, particularly elemental abundances, of the emitting regions observed and so help refine the existing theory of stellar evolution. The most likely possible sources were thought to include emission nebulae, at least very early O- and B-type stars, the coronas of cooler stars particularly of the red supergiant type, and novae. This list includes some of the more extreme examples of "population I" objects. Calculations based on a rather simple theory for quiet coronas (Grasberger and Henyey 1959), indicated that radiation from the chromosphere-corona of at least one of the nearby, bright supergiants (Deneb, Canopus, Betelgeuse, or Rigel) might be bright enough to be observed. The evidence presented below seems to indicate that a variety of stellar sources can be observed. The evidence also clearly indicates that for the detector sensitivities employed the Crab Nebula is not the most intense X-ray source in the night sky.

Data are presented in this article for the common portion of the sky scanned by counters carried aboard two different rockets. Results are labeled according to the energy interval and rocket flight, Nos. 4.69 or 4.70, discussed. A second article will give flight results for a relatively larger sky area (as shown by Fig. 9 below) which, however, was scanned by detectors aboard one rocket only. While both Aerobee-Hi sounding rockets were launched from Wallops Island, Virginia, the positions of celestial objects with respect to the earth, and its local magnetic field vector, were quite different for the two

* This work has been supported by the National Aeronautics and Space Administration under Contract NAS 5-1174 and by the Lockheed Independent Research Program.

flights. Consequently, for the portion of the sky considered in this paper, spurious effects arising from charged particles associated with the earth's magnetic field have presumably been minimized.

II. AEROBEE 4.69 DATA

The X-ray instrumentation consisted of a number of gas-proportional counters whose characteristics are given in Table 1. Counters with a middle initial "O" viewed the sky from the opposite side of the rocket than counters with a middle initial "E." Counters designated "K" were sealed units, while counters labeled "N" were gas-flow units. The counter filling was P-10 gas. A fairly detailed description of the detectors has been given (Fisher, Meyerott, Grench, Nobles, and Reagan 1963). Only one of the Table 1 counters, designated "N-E-65," failed to operate as designed. This failure is now attributed to

TABLE 1
AEROBEE 4 69 X-RAY DETECTOR CHARACTERISTICS

COUNTER LABEL*	ENERGY RANGE (keV)	COUNTER WINDOW			DETECTOR SOLID ANGLE	
		Area (cm ²)	Thickness (mg/cm ²)	Material	Degrees Maximum Aperture†	Probability of Count in Center Portion of Aperture‡
K-O-65	3-20	5 5	14	Be	6×80	0 5/20
K-O-90	3-20	5 5	14	Be	6×60	0 6/20
N-O-90	0 3-3	4 6	0 026	Formvar	60×90	1/80
K-O-115	3-20	8 0	23	Be	60×85	1/80
N-E-65	0 3-3	5 5	0 028	Formvar	6×80	0 5/20
K-E-90	3-20	8 0	23	Be	60×90	1/80
N-E-90	0 8-3	4 6	0 54	Mylar	24×60	1/50
K-E-115	3-20	5 5	14	Be	6×85	0 5/20

* The number in the counter designation gives the angle between the rocket and detector axis, measured from the rocket's tail

† The long dimension of the detector solid angle is parallel to the longitudinal axis of the rocket.

‡ Probability of a count being in the central portion of the solid angle's long dimension is given as (probability/degrees included in central portion).

the counter's gas reservoir being empty prior to launch. The pulse height of each detected event was telemetered to ground-receiving stations in order that an energy spectrum might be obtained for each source observed. To check absolute gain, each counter was exposed to 5.9 keV X-rays from a radioactive Fe⁵⁵ source. This check was made a number of times over a several-month period prior to launch, and for some 15 seconds on several counters about 1 minute after launch. A magnet to deflect low energy, at least up to 50 keV electrons, was placed near the input aperture of each counter to prevent such energy electrons from entering the counter.

Launch occurred on September 30, 1962, at an effective sidereal time of 1 hour, 36 minutes. A peak altitude of 173 km was achieved. The rocket was despun after launch to a rate of 16.4°/sec. Because the rocket's spin axis moved at a rate of 0.72°/sec around the surface of a yaw cone of 85.0° half-angle, a fairly thorough scan of the northern sky was obtained. The useful data-taking time, when the rocket was above 130 km, was several hundred seconds. Because the detectors possessed quite high sensitivity, ionospheric sounders were run during the day of the flight. The soundings showed no noticeable auroral activity at the time of the flight in the vicinity of the rocket's trajectory. Spread F was very slight and the lack of reflections from sporadic E regions indicated quiet ionosphere conditions. However, the sun was fairly active, a K_p value of 3 being

assigned the 3-hour interval containing the flight time; K_p values of 4 and 5 were reached before and after the flight.

The attitude of the rocket at each instant during the flight was initially (and roughly) determined from readings of a pair of magnetometers and finally (and accurately) determined from a pair of photomultipliers for observing visible-star light. While data from one of each kind of these aspect detectors would have been sufficient, pairs of these detectors were flown for reliability. The final X-ray counter aspect solutions are accurate to a little less than 1° in vehicle spin angle and 2° – 3° in the angle between the rocket's longitudinal axis and the center line of the X-ray detector's field of view.

The first step in the data-reduction process was to divide the range of telemetered pulse heights into intervals corresponding to 4 keV for the sealed counters and 0.5 keV for the flow counters. Intervals corresponding to about a factor of 2 in energy were selected for data analysis partly because of concern over absorption in the interstellar medium. Each set of data was smoothed in time by averaging the counts from three adjacent time intervals, counts in the center interval being weighted by a factor of 2 relative to counts in each of the side intervals. The time intervals used correspond to an angle (of rocket spin) representing about two-thirds of full width at half-maximum of the narrow dimension of a detector's angular field of view. Typical portions of actually observed data from two different counters for a little more than one complete spin of the rocket are shown in Figure 1. The results for the 12–20 keV interval have been plotted as actually observed and after being time-averaged and corrected for the counter's detection efficiency. This efficiency correction tends to produce occasional false peaks in counting rate because it emphasizes the occurrence of the 16–20 keV photons by a factor of two over the 12–16 keV photons. The counter-detection efficiency for 16–20 keV photons was about 10 per cent. Because of the very low counting rates involved, mere inspection of data like those shown in Figure 1 is not sufficient to locate celestial X-ray sources. The data from the poorly collimated detectors are the most difficult to interpret and have not been used for locating the emission regions discussed in this paper. For convenience, Figure 1 also gives the times when a detector scanned past several conceivable emission sources.

Figures 2 and 3 give plots of isophote contours for part of the Aerobee 4.69 data. To obtain these plots, data for a given counter were distributed on the celestial sphere and then were averaged over the common intersection of four adjacent sphere areas, each element of area having dimensions of one-third hour of right ascension and 2° of declination, as well as adjacent time intervals. Allowance for variation of detector sensitivity with angle, in a plane perpendicular to the direction of scan, as determined by laboratory measurements, was made by distributing the instantaneous count rates upon the celestial sphere in accordance with the prescriptions given in Table 1. The background level for each map was determined by arithmetically averaging the counts read from the dozen or so minimum count rate regions of each composite map. The lowest contour level given in Figures 2 and 3 represents a count level approximately one standard deviation, σ , of the (time- and area-averaged) background count above background. The blacked-in area gives the second contour level and represents a count rate 2σ above the background level. A dotted line is used for the 2σ contour level if not all individual detector count rates were 2σ above background. Because the count rates are very low, one standard deviation above background actually corresponds to levels $2x$, $2x$, and $2.5x$ the background level for the 1.5–2.5-, 4–8-, and 12–20-keV energy intervals, respectively. Specific flux values for the various contours of Figures 2 and 3 are given in Table 3 (see below). The dashed lines in Figures 2 and 3 encompass a region of the sky observed by detectors on Aerobee 4.70.

For each counter, scans contributing data within the dashed-line envelope were combined to give a single sky map. The nominal direction of all the used scans for all the counters was along a line of constant right ascension, at least for low declinations. Because the angular sensitivity of all counters was not very high, at right angles to the

direction of scan, the source declinations indicated in Figures 2 and 3 are believed to be more accurate than the right-ascension values. At declinations greater than about 64° , the extent of the common high-count-rate regions in the single-counter composite maps just described was reduced by use of sets of isophote plots composed of data from four successive scans. Sets of four passes were employed, because the combination of the large detector field of view and the manner of the rocket's precession produced quite extended area-emission regions in the composite map and so tended to obscure real source regions.

To further define the location of possible emission sources, contour maps obtained from different counters were combined. Figure 2, *b*, presents high-count-rate regions common to counters K-O-65, K-E-115, and K-O-90. Because of higher background, the latter counter was about four times less sensitive to 12–20-keV photons than the first

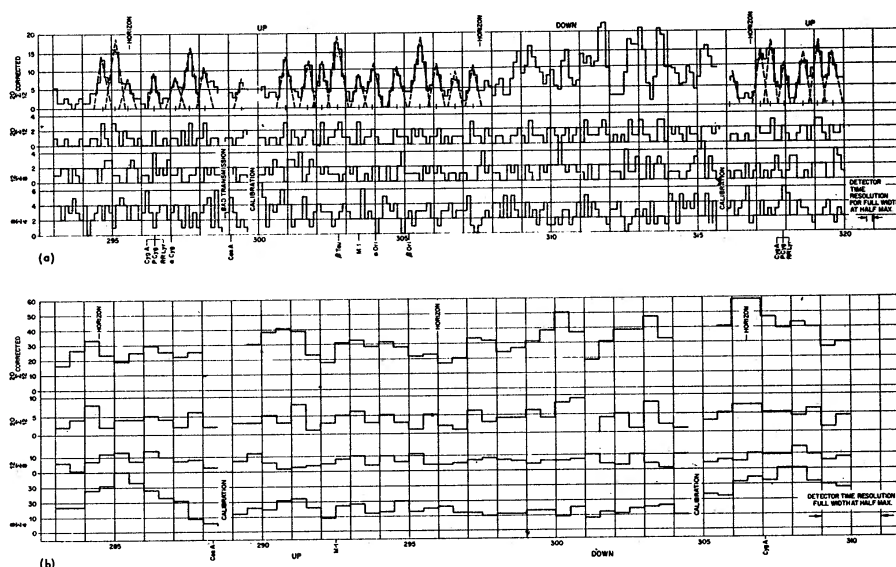


FIG. 1.—Typical Aerobee 4.69 detector telemetered data giving counts per unit time interval as a function of photon energy and time. Data for the 12–20-keV energy interval are given both as measured and after being time-averaged and detector-efficiency-corrected as described in the text. Tick marks on the time axis indicate when a detector was pointed directly at an object which might be capable of X-ray emission. *a*, K-O-65 data; *b*, K-E-90 data.

two counters listed. The simply outlined non-crosshatched portions of Figure 2, *b*, indicate the high-count-rate regions common to counters K-O-65 and K-E-115 only. The 4–8-keV photon emission regions presented in Figure 3, *b*, are common to six successive scans of the sky made by counters K-O-65 and K-O-90. As indicated by the second initial of their labels, both of these detectors viewed the sky from the same side of the rocket. Location of source regions at declinations of 70° to 85° adjacent to the very top of Figures 2 and 3 near a right ascension of 18 hours may ultimately be better defined by use of data obtained very early in the flight. The very early scans were made in a direction nearly perpendicular to that of the rather later scans whose data were used for the figures.

Some of the Aerobee 4.69 data have also been analyzed by other methods than that just described. One procedure amounted to location of portions of the celestial sphere common to a number of fields of view of several different counters. The center of each of these fields of view was defined to occur at the time of count-rate maximum as determined from information like the tick marks on the time axis of the K-O-65 efficiency-corrected 12–20-keV photon flux shown in Figure 1, *a*. The most detailed map prepared in this manner utilized the 12–20-keV results from detectors K-O-65, K-E-115, and

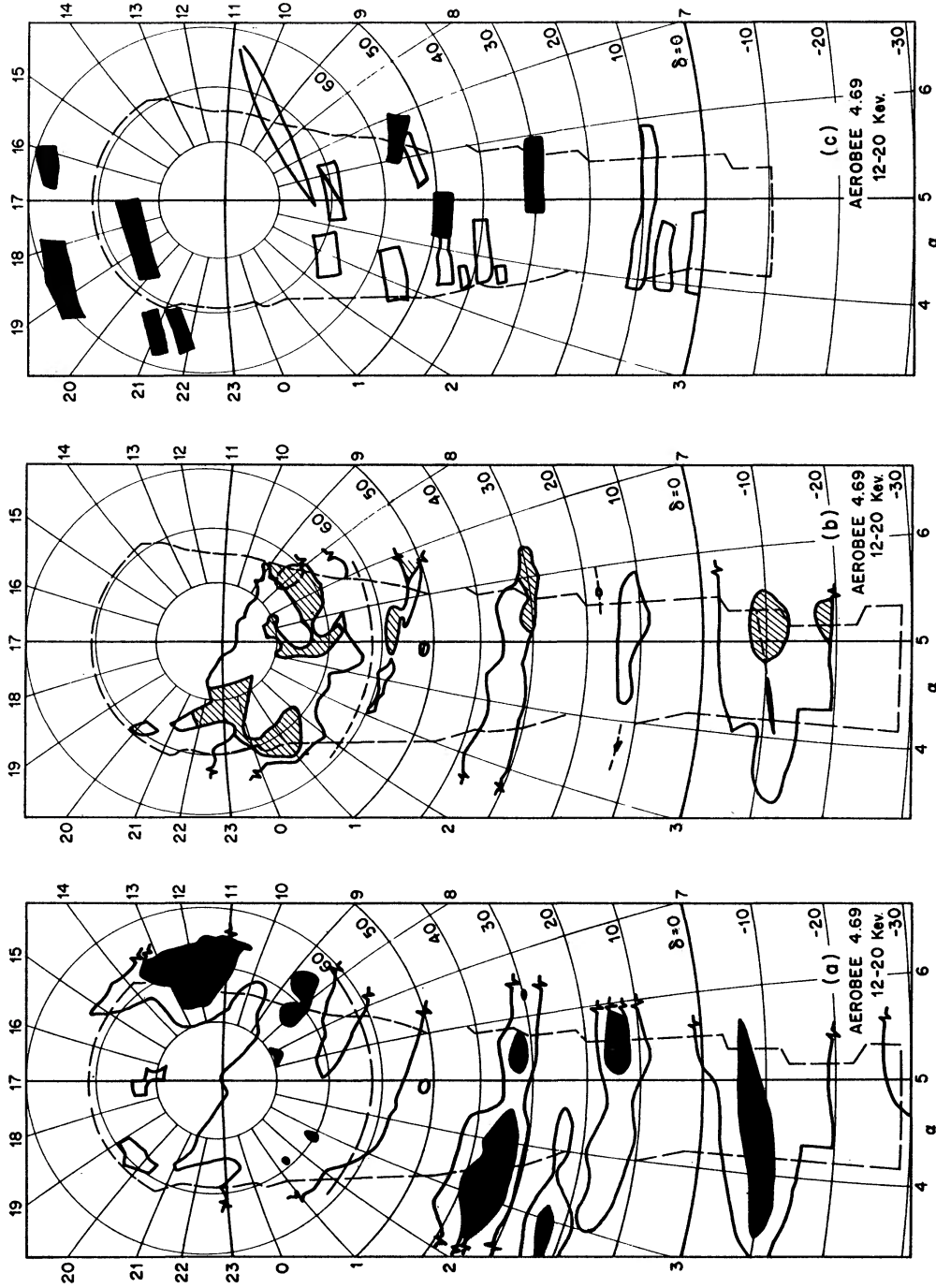


FIG. 2.—Apparent emission regions of 12-20-keV photons. *a*, isophote plot of the data for detector K-E-115; *b*, high-count-rate regions common to isophote plots of detector K-E-115 and K-O-65 data, the region being crosshatched if it also coincided with a high-count-rate area from a K-O-90 isophote plot; *c*, regions having simultaneous count-rate maxima in the portion of the field of view shared by detectors K-O-65 and K-O-90, on two successive scans. The region is black if it was observed on three successive scans.

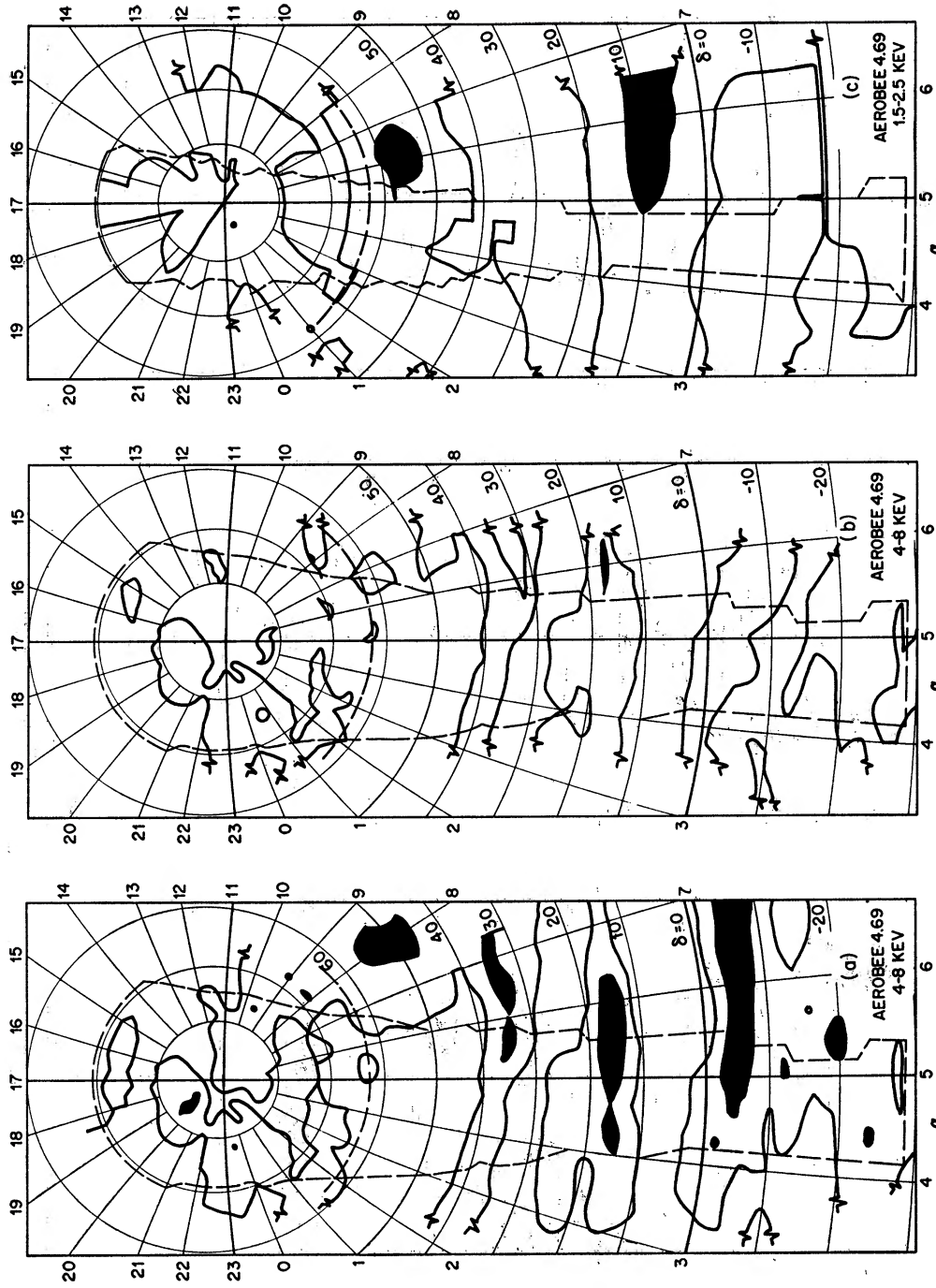


FIG. 3.—Isophote plots of apparent emission regions of low-energy photons. *a* and *b*, regions of 4–8-keV photon emission as observed by detectors K-O-90 and K-O-65, respectively; *c*, N-E-90 detector results.

K-O-90. Over half of the 12–20-keV regions found to be common to the fields of view of these three detectors were the same as those found by employing the isophote contour methods used for Figures 2, *b*, and 3, *b*. Common region boundaries were nearly the same for the two methods of analysis.

Still another analysis procedure was based on determining fields of view common to counters K-O-90 and K-O-65, when each had a maximum in 12–20-keV photon count rate within a time corresponding to about one-half of the field of view of either counter. Figure 2, *c*, indicates the results of such a comparison. The portion of data examined in terms of both common field of view and coincidence in time appeared ultimately to yield the same source locations as did the data studied only in terms of common field of view.

The large acceptance angles of the various counters and the relatively large number of high-count-rate regions suggests that some of the regions of Figures 2 and 3 may either encompass or else lie between a small set of close emission sources. A combination of this and the few counts above background associated with individual regions of high-count rate indicates that the photon flux assigned to the different counter levels is really not very well determined. Inspection of the original telemetered count records, like those in Figure 1, shows that the procedure for determining common regions based on isophote plots places such a high value on each individual count that a given counter scanning over a potential high-count-rate region will rarely sense a noticeably high number of counts on all of the opportunities available to do so. Probably the contour levels are trustworthy to within about a factor of 3. Because of the various calibrations performed, errors in photon energy of ± 30 per cent and ± 20 per cent are assigned to the data from the N- and K-labeled counters, respectively.

At least one terrestrially associated source of 4–8-keV photons may have been found. This source is identified with the large count-rate peak in Figure 1, *b*, near 285 sec. The source appears on five successive spins of the rocket and seems to lie quite near the northern horizon. Whether the emission comes from a celestial region near but actually above the horizon, from a geocorona, from an auroral effect, or from Russian nuclear-device debris created several days prior to the rocket flight is not now apparent. But the 4–8-keV counting rate, as obtained from detectors K-E-90 and K-O-115, is about ten times higher than that of any other source region. In view of the 5-msec duration of each telemetered pulse, proper allowance for loss of counts would make the peak rates near 286 sec some 30 per cent higher than shown in the figure.

III. AEROBEE 4.70 DATA

The high counting rates and large number of apparent source regions observed by Aerobee 4.69 detectors caused reduction of the data to be quite difficult. Consequently, a somewhat smaller field of view and a plastic scintillator plus a photomultiplier-anticoincidence shield was used for each Aerobee 4.70 detector. The magnetic field employed to prevent electrons from entering the counter was also made stronger so that electrons less energetic than 75 keV were suppressed. These three improvements produced an increase in X-ray detection sensitivity amounting to factors of about 2, 2, and 10 for the 12–20-, 4–8-, and 1–2.5-keV photon energy intervals, respectively.

Characteristics of the four different detectors flown on Aerobee 4.70 are listed in Table 2. Each counter possessed a 5-cm² aperture. The thin windows of counters K-A-115 and N-B-115 were both ruptured during rocket launch. The gas in sealed-counter K-A-115 leaked through the broken window, and so no usable data were obtained. In spite of flow-counter N-B-115's broken window, the quantity of gas stored in the counter's reservoir was sufficient to allow data to be taken for about two-thirds of the flight. Instrumentation for determining rocket attitude was similar to that carried on Aerobee 4.69.

The rocket was launched on March 15, 1963, at an effective sidereal time of 8 hours, 50 minutes. Peak altitude for the flight was 197 km. One minute after launch the rocket was despun to about 15°/sec. In spite of the 50° half-angle yaw cone of the rocket's spin

axis, the small $0.18^\circ/\text{sec}$ precession rate of the spin axis on the yaw cone's surface resulted in only a relatively small portion of the available sky being scanned. Surveillance by the MIT Ionosphere Station, Westford, Massachusetts, was added to that provided previously by the CRPL stations at Wallops Island and Fort Belvoir, Virginia. No particular auroral activity occurred during the flight, either in the vicinity of the rocket's trajectory or near the rocket's northern horizon. In contrast to the Aerobee 4.69 launch, solar activity was quite low, and K_p for the 3-hour interval containing the launch time was 2. For 12 hours both before and after launch, K_p values of 1 prevailed.

Figure 4 presents counts for detector K-B-90 which were obtained for the same portion

TABLE 2
AEROBEE 4.70 X-RAY DETECTOR CHARACTERISTICS

COUNTER LABEL*	ENERGY RANGE (KEV)	COUNTER WINDOW		DETECTOR SOLID ANGLE (DEGREES MAXIMUM APERTURE)†
		Thickness (mg/cm ²)	Material	
N-A-90	0.6-4	0.54	Mylar	10×20
K-A-115	3-20	14	Be	10×20
K-B-90	3-20	23	Be	10×20
N-B-115	0.6-4	0.080	Formvar	10×20

* The number in the counter designation gives the angle between the rocket and detector axis measured from the rocket's nose.

† The long dimension of the detector solid angle is parallel to the longitudinal axis of the rocket. A probability of 0.66 exists for the count being in the center 14° of the 20° dimension.

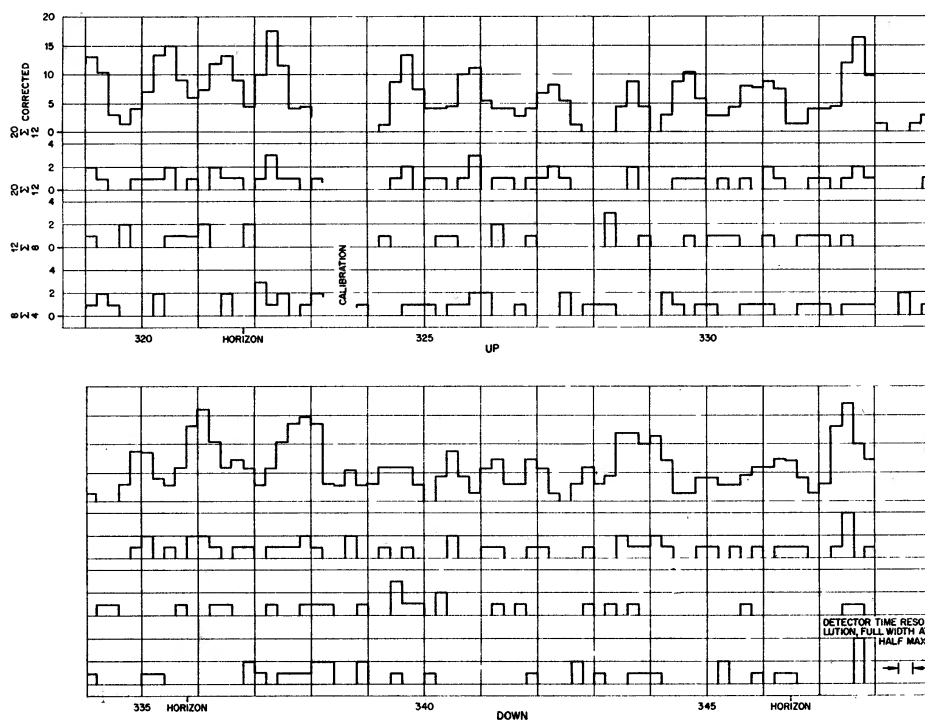


FIG. 4.—Typical portion of telemetered data for detector K-B-90. Data for the 12–20-keV energy interval are given both as measured and after being time-averaged and detector-efficiency-corrected as described in the text.

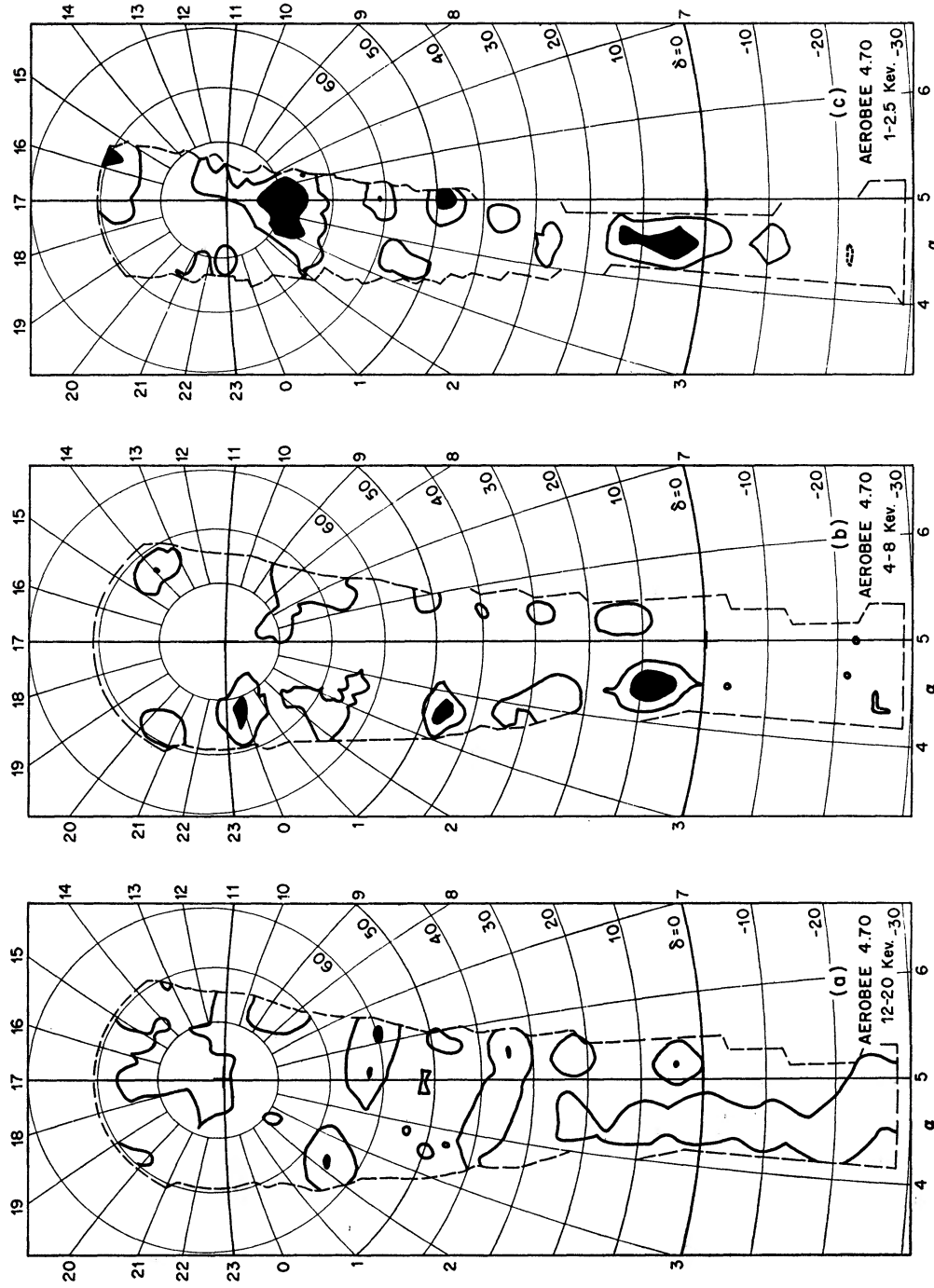


FIG. 5.—Isophote plots of regions apparently emitting various energy photons. α and b , derived from detector K-B-90; c , data from detector N-A-90.

of the sky as the counts given in Figure 1. At 331.4 sec, the detector scanned past the Crab Nebula. With one exception, Aerobee 4.69 data-reduction procedures were simply carried over to the second flight's data. This exception amounted to combining into one isophote plot all the scans of the sky made for a given energy interval and detector. The relatively small counter field of view and the small amount of rocket precession made this combination feasible. Isophote plots for the portion of the sky scanned by detectors K-B-90 and N-A-90 are given in Figure 5. The second letter in the counter label indicates that these two detectors observed the sky from opposite sides of the rocket. The qualitative remarks concerning the accuracy of isophote contours of Aerobee 4.69 data can also be applied to Aerobee 4.70 data. That is: (a) the size of the detector field of view makes

TABLE 3
FLUX LEVELS FOR CONTOURS GIVEN IN VARIOUS FIGURES

FIGURE	ENERGY INTERVAL (KeV)	PHOTON FLUX (photons/cm ² -sec-keV)	
		Background	1 σ Contour (Flux above Background)
Aerobee 4 69			
2, <i>a</i> and <i>b</i>	12-20	0 19	0 28
3, <i>a</i> and <i>b</i>	4-8	0 14	0 14
3, <i>c</i>	1 5-2 5	3 6	3 6
Aerobee 4 70			
5, <i>a</i>	12-20	0 11	0 16
5, <i>b</i>	4-8	0 45	0 68
5, <i>c</i>	1-2 5	0 17	0 25
Intercomparisons			
6, 7, 8, 9		Use Aerobee 4.70 values from Figure 5	

accurate location of an emission source quite difficult, (b) the precise values of the flux contours are really not well known, and (c) for a given emission region a high-count rate is not always obtained when a detector scans over the region. Errors in photon energy of ± 50 per cent and ± 20 per cent are assigned to the data from the N- and K-labeled counters, respectively. Specific flux values for the various contours shown in Figure 5 are given in Table 3.

With the data reduction procedures used, X-rays appear to arrive from a sizable fraction of the sky. If the rocket's behavior in providing only a limited scan of the sky had been known prior to the flight, differently dimensioned fields of view would have been used.

IV. X-RAY EMISSION REGIONS

a) Location

Data from the two rocket flights have been intercompared on the basis of a common energy interval. As mentioned in the introduction, such a comparison might be expected

to diminish the effect of difficulties caused by terrestrially associated X-ray sources. Because of the slightly higher sensitivity of Aerobee 4.70 detectors, any real regions of high relatively time-independent flux seen by Aerobee 4.69 detectors should have been seen by Aerobee 4.70 counters. Figure 6 presents results for the two highest energy intervals investigated. The 1–2.5-keV interval data are not shown because of the low angular resolution of the Aerobee 4.69 flow counters. Figure 5, *c*, data, from Aerobee 4.70 only, must be relied on for the lowest energy interval. Each region of Figure 6 had a count rate of at least 1 standard deviation above the background rate (of the time and celestial-sphere area averaged data) applicable to each of the counters involved in the data from the individual flights. Table 3 lists the photon flux levels corresponding to the different contours of Figures 6–9. Because of the nearly unit detection efficiency for 4–8-keV photons, isophote contour data for this energy interval are of higher quality and hence should be more trustworthy than data for either the 1–2.5- or the 12–20-keV energy intervals.

Locations of the emission regions given in Figures 2, 3, 5, and 6 are intercompared in Figures 7–9. Validity of the results given in the latter figures is based on the assumption, unnecessary and so avoided thus far, that interstellar absorption effects are negligible for the photon energies whose emission regions are being compared. Figure 7, *a*, was obtained from Figures 2, *b*, and 3, *b*, each of which indicated a high count rate in two different energy intervals from detectors aboard Aerobee 4.69. Figure 7, *b*, represents Aerobee 4.70 data and was derived in a similar manner to that used for Figure 7, *a*. As expected, the Aerobee 4.70 detector indicates more high-count-rate regions than the less sensitive Aerobee 4.69 detectors. Figure 7, *c*, was derived by comparing Figure 7, *a* and *b*. As expected, the same Figure 7, *c*, regions appear if the data of Figure 6, *a* and *b*, are compared.

Figure 8, *a* and *b*, presents regions associated with emission of 1–2.5-keV and 4–8-keV photons. Because of the fairly wide-open collimation used on the lowest energy Aerobee 4.69 detectors, Figure 8 regions were derived without the use of the N-E-90 results given in Figure 3, *c*. A third set of emitting areas can be obtained by determining Aerobee 4.70 observed sources of 1–2.5- and 12–20-keV photons which are not associated with 4–8-keV photons. Figure 8, *c*, indicates these regions. Presumably all of these regions should be viewed with suspicion because a valid physical explanation of such an unusual emission spectrum seems quite difficult.

Of the fifteen different Figure 8, *c*, locations shown, the simple outline for ten of the areas indicates their apparent association with 4–8-keV emission measured on one or the other of the two flights. Six of the ten areas being related to Aerobee 4.70 data, while the remaining four locations are for Aerobee 4.69 data. Of the ten regions, several are also associated with 12–20-keV photons. Two simple interpretations of the remaining five regions (blackened in Fig. 8, *c*) can be made, the first being merely that all such regions are spurious and indicate the quantity of regions which can arise from accidental superpositions. The second interpretation is that the crosshatched regions in Figure 8, *c*, are real and appear because of the high importance assigned to the few photons detected. Arguments based on the count in a region being so many standard deviations above the background count can really be applied with confidence only to the relatively large number of photons detected in the 4–8-keV interval. The proper viewpoint from which to consider the five remaining regions shown in Figure 8, *c*, is presumed to lie somewhere between the two extreme interpretations just given.

It is interesting to note that only two of the 1–2.5-keV Aerobee 4.70 indicated-emission regions at ($\alpha = 3^{\text{h}}30^{\text{m}}$, $\delta = +56^{\circ}$) and ($\alpha = 5^{\text{h}}$, $\delta = +45^{\circ}$), are apparently not associated with either 4–8- or 12–20-keV photons. The first of these regions lies on the galactic equator near several distinct dark nebulae, and the second region encompasses the location of α Aur.

Several crude measures of the reliability of the data have been attempted in addition to that shown by Figure 8, *c*. The simplest estimate of how many common sky regions

might appear is obtained by considering all count-rate peaks to be occurring in a purely random manner in time. Inspection of data for a single scan of the sky by an Aerobee 4.69 detector, from which results like those shown in Figure 2, *c*, were obtained, sets an accidental rate of occurrence of maxima in 12–20-keV photon count rate of a single counter as about two per second. The resolving time of the counters (due to the rocket's spin) was about one-fifth second. The expected rate of purely accidental coincidences of fields of view is therefore about $\frac{1}{3}$ per second for a sixfold coincidence. On this basis one or two accidentally occurring common regions might be expected for the part of the sky shown in Figure 2, *c*. Actually some half-dozen regions seem to satisfy the sixfold coincidence requirement.

Still another manner of determining data reliability is to search for common fields of view in the downward direction. Positions of count-rate maxima are plotted in celestial-sphere coordinates just as if the earth were not present. The principal difficulty inherent in this procedure is the experimentally observed fact (see Fig. 1, *a*) that at least in the

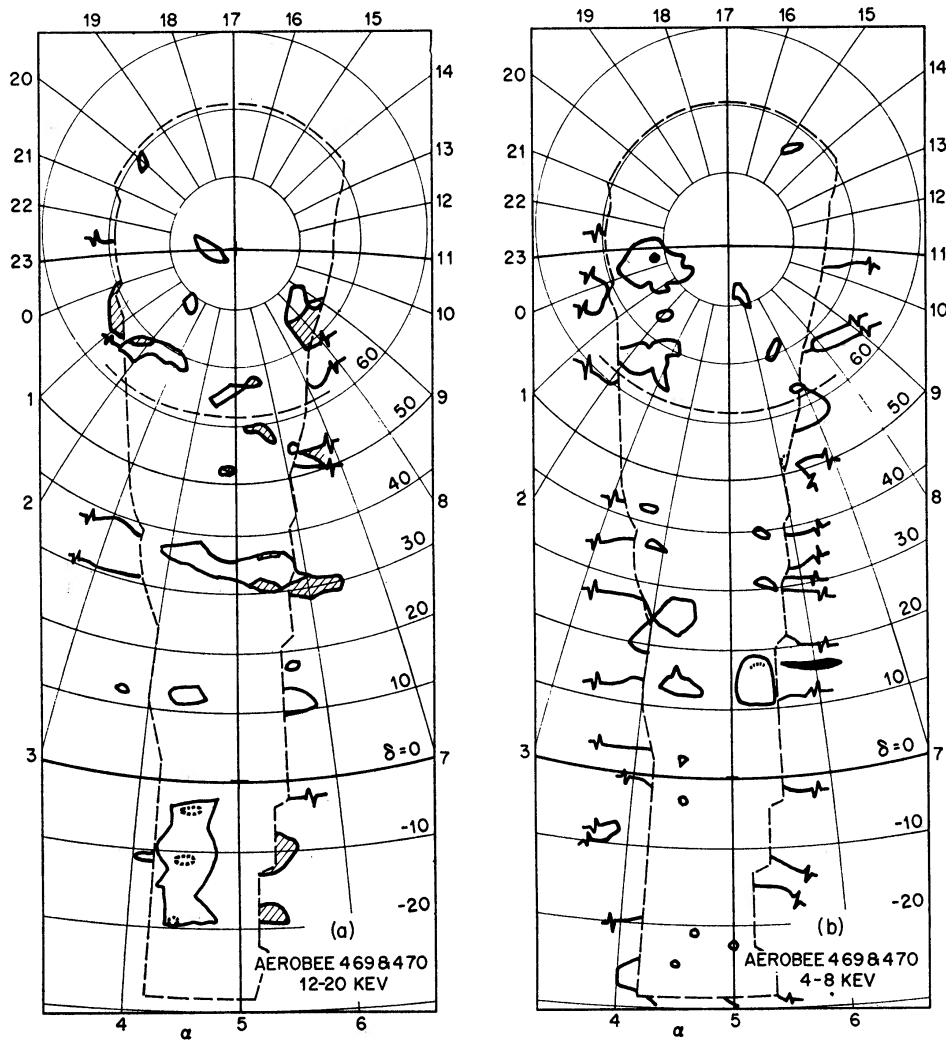


FIG. 6.—High-count-rate regions common to isophote plots of detectors aboard Aerobee 4.69 and 4.70. Lines protruding from the Aerobee 4.70 scanned portion of the sky indicate Aerobee 4.69 data given in earlier figures.

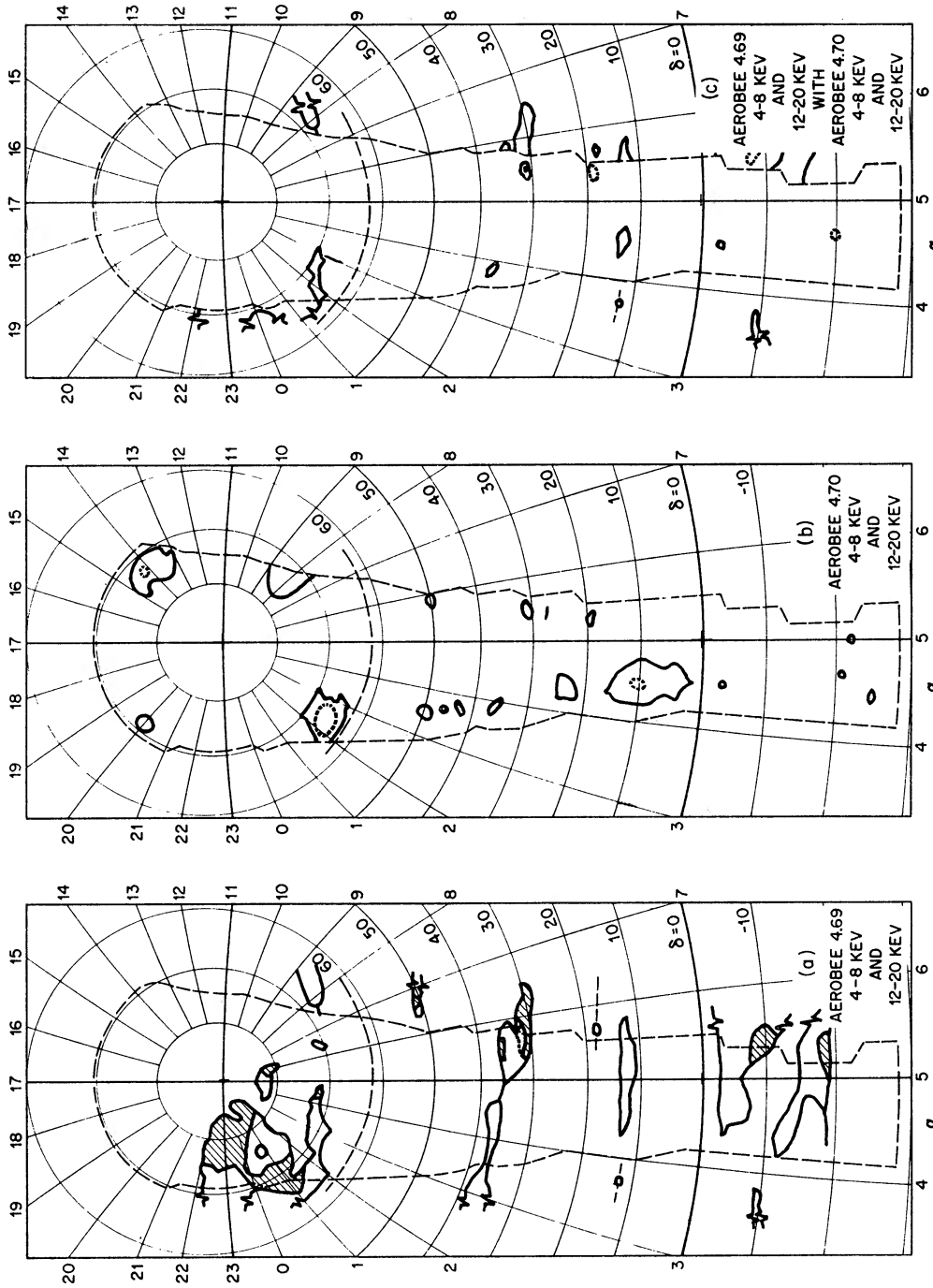


FIG. 7.—Apparent emission regions of 4-8- and 12-20-keV photons obtained from previous isophote plots. *a* and *b*, comparisons of different energy-interval regions obtained from Aerobee 4.69 and 4.70 data; *c*, regions common to both 4-8- and 12-20-keV photons observed on each of the two flights. The two broken outline regions show possible additional source locations.

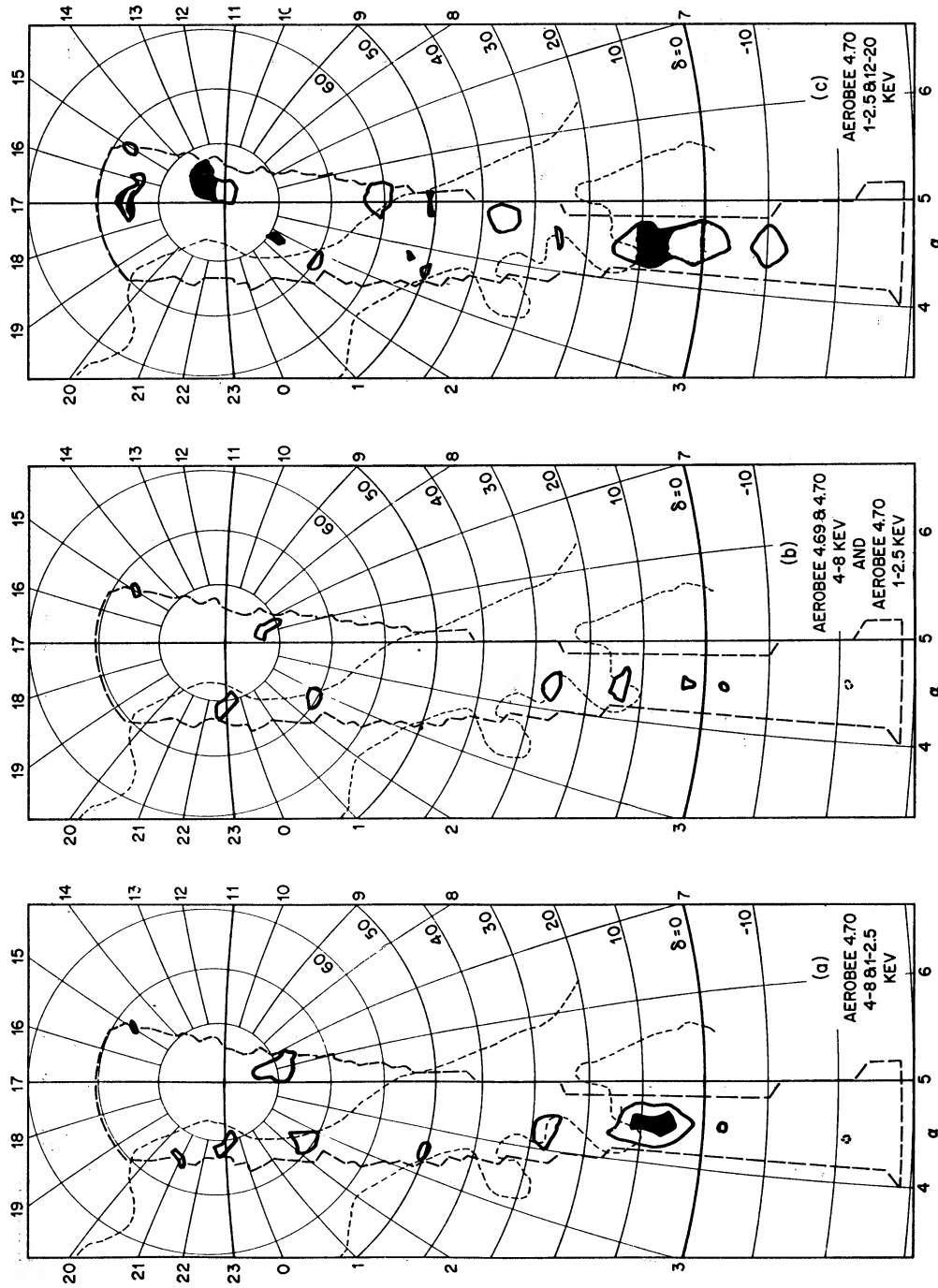


FIG. 8.—Apparent emission regions of low-energy photons obtained from previous isophote plots. *a*, Aerobee 4.70 data only; *b*, derived by intercomparing the 4–8-keV emission regions measured on Aerobee 4.69 and 4.70 and then determining areas also associated with 1–2.5-keV photons observed during the Aerobee 4.70 flight; *c*, Aerobee 4.70 determined regions having high-count rate for 1–2.5-keV and 12–20-keV photons and not associated with 4–8-keV photons observed by Aerobee 4.69 or 4.70 detectors. The diagonal dashed lines in the figure represent Hubble's (1936) zone of avoidance.

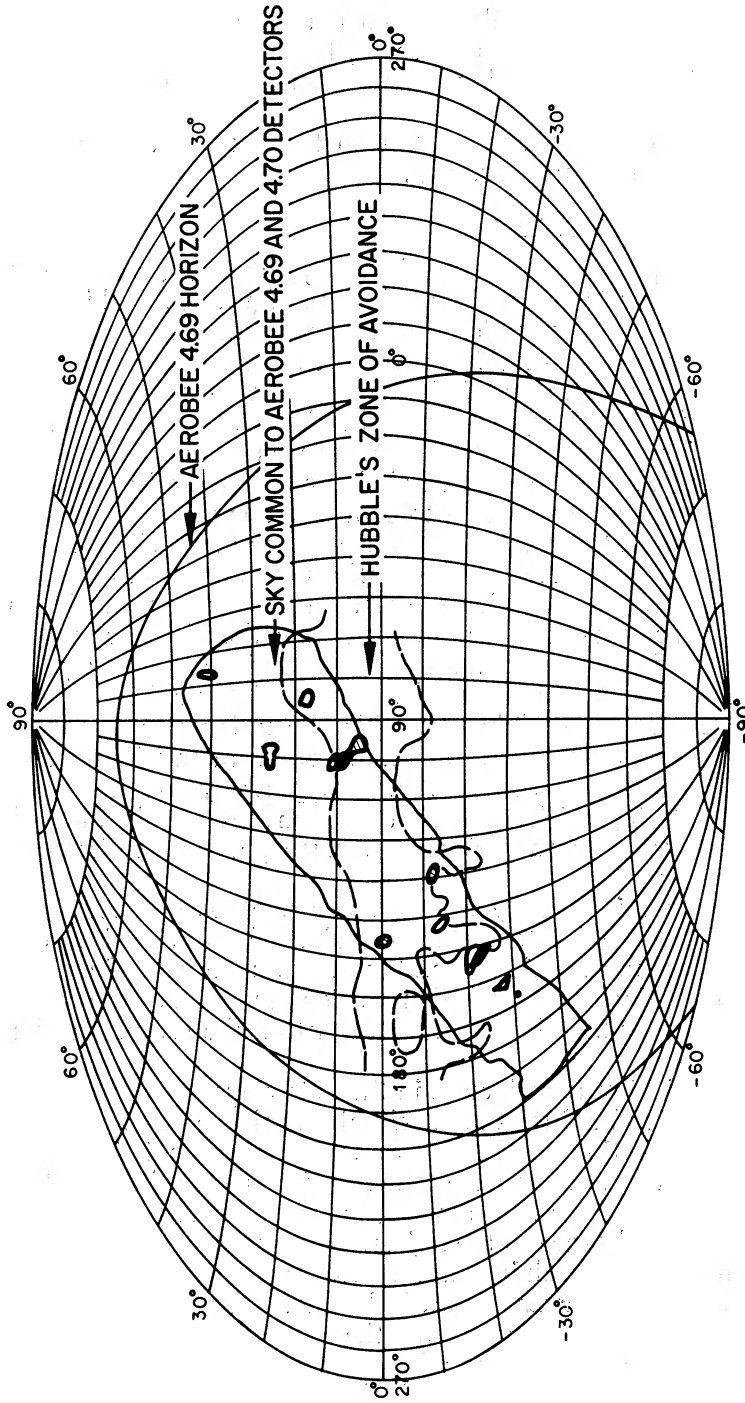


FIG. 9.—Galactic coordinate plot (old system) of common regions observed to have high-count rate for different energy photons as found from isophote plots for data in each photon-energy interval. The crosshatched regions appeared to emit photons in the 4-8- and 12-20-keV energy intervals during each of the two rocket flights. The simply outlined regions appeared to emit 4-8-keV photons during both flights as well as 1-2.5-keV photons during the Aerobee 4.70 flight. Black regions are those found common to the crosshatched and simply outlined areas and occur at latitudes of $+9^\circ$, -23° , and -31° .

12–20-keV interval the highest count rate per field of view occurs when the counter is looking down toward the earth. As a result more accidental coincidences are found downward than upward and so any real night-sky sources are treated with more than the proper amount of suspicion. To date only a small portion of the downward sky for Aerobee 4.59 data has been examined. As expected, the number of common emission regions found downward is higher per unit sky area than when the sky away from the earth is being observed.

For the reasons given above it would seem that at least half of the high-count-rate regions discussed below and in Figure 9 are real.

b) Tentative Source Identification

Data based on Figure 6, *b*, and presented in Figures 7, *c*, and 8, *b*, constitute the final results of the experiments and so have been combined in Figure 9. Any high-count-rate region indicated was noticed at the very least by two different rocket flights. Further, each region was observed in the 4–8-keV interval which is considered (because of the higher number of counts measured) to contain inherently the most reliable data. A tentative attempt at identification of the regions shown in Figure 9 is given in Table 4, emphasis having been placed on individual rather than groups of stars. The table also lists a number of other positions, several apparently being associated with X-ray emission if the results of only one flight are considered to be acceptable proof. The remainder of these other positions correspond to the brightest stars of Allen (1955). The number given for the frequency of Aerobee 4.70 detector observations corresponds to the fraction of total scans over a source position on which the count rate was 1σ above background. Because the fraction for each location was obtained from the highest nearby contour level shown in the data of Figure 5, the number of opportunities to scan a given object sometimes appears (incorrectly) to depend upon the energy interval being investigated. There are three principal reasons for giving the table: (1) to indicate that a variety of stellar objects lies near regions which seem to emit detectable quantities of soft X-rays; (2) to imply that objects emitting 12–20-keV photons apparently do not always possess the highest absolute magnitude; and (3) to show that count-rate maxima in a given detector's data are not always observed each time a given potential emission region is scanned.

The last-named situation arises partly from the few photons measured and partly from the division of an Aerobee 4.70 detector's angular field of view into only three portions. A fourfold decrease in detection efficiency occurs upon going from the center to the edge of the central portion of the field of view. Consequently, only a rather bright source could be observed every time it fell anywhere within the central portion of the field of view.

The objects listed in Table 4 were arrived at in the following manner. Any individual object was considered if it was brighter than a visual magnitude of 6.2 and fell within about a 100-square-degree portion of the sky centered on an emission region. The "brightest nearest" objects in the table were found by intercomparing absolute visual magnitudes of the individual objects and allowing for the observed visible flux to fall inversely as the square of the distance to the object. Wherever possible, parallax values of Jenkins (1952) were used. The remaining parallax values and the absolute magnitudes were taken from Allen (1955) or Becvar (1960). Only the two or three brightest objects found in this manner are given in the second from the last column of the table. "Other" objects with interesting physical properties and suitable position coordinates are listed in the last column. Interesting properties arbitrarily include objects with magnetic fields, intrinsic and eclipsing types of variables, novae, emission nebula, dark nebulae, and external galaxies. HD numbers are used for objects listed in any of the four tables of Babcock's (1958) magnetic star catalog, unless the object is so bright as to have a Greek letter designation. Several 3C sources (Edge, Shakeshaft, McAdam, Baldwin, and Archer

TABLE 4
 POSSIBLE IDENTIFICATION AND FREQUENCY OF OBSERVATION OF SOME OF THE
 REGIONS ASSOCIATED WITH X-RAY EMISSION

LOCATION		FREQUENCY OF AEROBEE 4.70 OBSERVATIONS IN DIFFERENT ENERGY INTERVALS*			POSSIBLE IDENTIFICATION	
		12-20	4-8	1-2.5	Brightest Nearest	Other
α	δ					
Regions Observed in 4-8 and 12-20-keV Intervals on Both Flights						
2 ^h 20 ^m	+65°	3/4	4/4	O	ϵ Cas, † HD 15089, ω Cas	Dark nebulae, HD 10221, IC 1747
2 30	+70	3/4	2/5	4/5	<i>HD 15089</i>	RZ Cas, SU Cas
4 0	+36	3/6	3/5	0/5	<i>H-II</i> (ξ Per), ϵ Per, ω Per	Dark nebulae, 49 Per, NGC 1579, AG Per, HD 25354, IC 351, IC 2003
4 30	+12	4/7	6/7	4/6	α Tau †, π_2 Ori, <i>90 Tau</i>	μ Tau, HD 29140, R Tau, λ Tau
4 30	- 3	4/8	4/9	3/6	ν Eri, μ Eri, ξ Eri	NGC 1637, NGC 1788
5 30	+30	1/2	2/2	O	β Tau †, χ Aur	Dark nebulae, <i>T Aur</i> , U Aur, 3C 111, H-II (IC 410)
Regions Observed in 4-8-keV Interval on Both Flights and 1-2.5-keV Interval on Aerobee 4.70						
2 30	+70				See above	
4 20	+27	5/8	6/7	3/6	τ Tau, ϕ Tau, HD 25823	<i>IC 2087</i> , IC 359, dark nebula, RY Tau, RV Tau, TT Tau, 3C 123
4 30	+12				See above	
4 30	+ 3	4/8	6/7	4/6	<i>45 Eri</i> , 49 Eri, 44 Eri	π_5 Eri
4 30	- 3				See above	
6 10	+82	0/5	5/5	3/4	<i>NGC 9073</i>	NGC 2146, NGC 2268, NGC 2336, VZ Cam, SV Cam, SY Cam, NGC 8574
15 0	+74	2/3	4/4	3/3	β U Mi †	γ U Mi, 4 U Mi, 5 U Mi, V U Mi
23 0	+79	0/3	3/5	2/3	γ Cep, 34 Cep, 31 Cep	π Cep, 23 Cas, V Cep, HD 215038
Other Positions Scanned						
1 22	+89	2/4	1/4	2/3	α U Mi †	
3 30	+50	2/5	3/5	2/4	α Per †, δ Per, 31 Per	29 Per, IQ Per
5 9	+46	1/4	1/4	2/3	α Aur †	
5 10	- 8	0/2	1/2	O	β Ori †	
5 20	+ 6	1/2	1/2	O	γ Ori †	
5 30	- 1	1/1	1/1	O	δ Ori †, ϵ Ori †, ζ Ori †	
5 53	+37	0/2	1/2	O	θ Aur †	
5 52	+45	1/2	0/2	O	β Aur †	

* Fractions indicate the total number of scans over an object when the count rate was 1σ above background. An O indicates the region was not scanned by the detector sensitive to 1-2.5-keV photons.

† Italicized objects have a position which gives the best agreement with an emission-region location.

‡ Allen's list of 100 brightest stars

1959) having 0.1–1 per cent of the 960 Mc/sec radio flux of Cassiopeia A are given in Table 4. The brightest radio source near an X-ray emission region is 3C 123. Actually several dozen other weaker 3C radio sources lie near areas shown in Figure 9.

A differently motivated identification procedure was also tried, namely, correlation of source regions on the basis of a given physical property. Partly because of the very small number of identified source regions, no statistically significant correlation seems possible now.

The position errors inherent in the Figure 9 regions can be fairly easily grasped by referring back to Figure 7, *c*. The error in the precise location and size of an emission area is such that β Tau at ($\alpha = 5^{\text{h}}23^{\text{m}}$, $\delta = +29^{\circ}$) might actually lie within an accurately drawn perimeter for the ($\alpha = 5^{\text{h}}30^{\text{m}}$, $\delta = +30^{\circ}$) location. In comparison to β Tau, the Crab Nebula lies about twice as far away from a labeled region. The larger dimension of a detector field of view was so oriented that the right ascension for a source location is less well known than the declination. Consequently α Tau at ($\alpha = 4^{\text{h}}33^{\text{m}}$, $\delta = +16\frac{1}{2}^{\circ}$) may actually lie within the emission region at ($\alpha = 4^{\text{h}}30^{\text{m}}$, $\delta = +12^{\circ}$).

TABLE 5

CALCULATED 2–8-Å LUMINOSITY FOR SOME OF THE OBJECTS ITALICIZED IN TABLE 4 THAT ARE ASSOCIATED WITH 1–2.5-KEV EMISSION REGIONS OF AEROBEE 4 70 DATA

OBJECT ITALICIZED IN TABLE 4	FLIGHTS OBSERVED FOR ENERGY INTERVAL GIVEN		APPROXIMATE VALUES OF		2–8-Å LUMINOSITY/TOTAL SOLAR LUMINOSITY*	
	12–20 keV	4–8 keV	Distance (pc)	M_v	Simple Ratio	Ratio Altered by Visual Luminosity Difference
HD 15089	Both	Both	50	1	0 15	0 005
α Per	4 70	4 70	140	–4	1	0005
90 Tau	Both	Both	40	1	0 1	002
45 Eri	4 70	Both	140	–1	1	006
ν Eri	Both	Both	300	–3 5	6	.004
α Aur	Neither	Neither	150	–0 5	<1	< 01
NGC 9073	4 69	Both	60	1	0 2	006
β U Mi	4 70	Both	30	0	0 05	0005
γ Cep	4 69	Both	16	2 5	0 15	0 02

* A flux detection sensitivity of $\sim 2 \times 10^{-9}$ ergs/cm²-sec has been assumed

Of the four supergiants mentioned in Section I, only Rigel was scanned on both flights. Although Rigel does lie within a high-count-rate region of Figure 7, *a* (for Aerobee 4.69 data), it does not appear that Rigel was observed on either of the two possible occasions during the Aerobee 4.70 flight. Whether this is evidence for a time variation in the source star or on improper identification of a first-flight emission region is not now apparent, although the presence of the Trapezium in the Aerobee 4.69 emission region containing Rigel should be noted.

c) 2–8-Å Luminosities

Efforts described so far have amounted to comparing the data from detectors possessing a variety of energy and angle sensitivities in order to locate X-ray emission regions which might be common to a number of scans of the night sky. By resorting solely to Aerobee 4.70 data, because these detectors had the best sensitivity and identical collimation systems, approximate luminosities can be derived for the regions of apparent emission common to both flights. Table 5 presents information about the lower-energy photon sources located in Figure 8, *b*.

The detection sensitivity of about 2×10^{-9} ergs/cm²-sec for photons in the 2–8-Å interval established the level of an object's X-ray emission. Table 5 gives the luminosities calculated for most of the objects italicized in Table 4 that are associated with low-energy photons. The small number of observed emission regions and the error in source location is such that no valid basis now exists for selecting any object from Table 4 other than that arbitrarily associated with both the best location and highest absolute luminosity. While the value found for an individual object is not considered very trustworthy, the range of luminosities is considered worth notice. This follows from the fact that within factors of 10–100, the same luminosity is obtained for most of the eligible objects near a given source location. For comparison with the sun, a quiescent solar flux of 10^{-4} ergs/cm²-sec above 1.5 keV has been assumed. This value was inferred from the recent measurements made by Pounds, Willmore, Bowen, Norman, and Sanford (1963) and establishes that of the order of 10^{-10} of the total quiescent solar luminosity appears in the form of 2–8-Å photons. As the solar X-ray spectrum above 1 keV varies quite rapidly with photon energy, at best only a crude comparison of stellar and solar X-ray emission can be made. Two kinds of comparison are given, the first allowing only for the distance to the star, the second allowing for the distance and also the difference in absolute visual magnitude. If the sun were presumed to be, in terms of X-ray data, the most active of all objects, a valid comparison might lie somewhere between these two extremes. Actually the values in Table 5 indicate that, by a factor of as much as 10^6 , the quiescent sun is not the most copious stellar emitter of 2–8-Å photons. To invalidate this conclusion, at least the six emission-region locations associated with both flights shown in Table 5 must be proved spurious.

d) *Supernova Remnant Observations*

The Crab Nebula certainly appears to be less bright at the X-ray energies measured in this experiment than other celestial objects. From the two applicable Aerobee 4.70 scans, limiting intensities of flux in the 4–8-keV and 12–20-keV energy intervals are set at 0.07 and 0.3 photons/cm²-sec-keV, respectively. These values correspond to the 1σ contour of data shown in Figure 5, *a* and *b*. No Aerobee 4.70 N-A-90 detector scans of M-1 were made at a sufficiently high altitude to yield reliable data. Consequently data from the less sensitive Aerobee 4.69 detectors must be used for the 1.5–2.5-keV photon energy interval. The 1σ contour from detector N-E-90 results given in Figure 3, *c*, would set the 1.5–2.5-keV flux as less than or about 3.6 photons/cm²-sec-keV.

Both Cassiopeia A and Cygnus A were scanned by Aerobee 4.69 detectors. Limiting fluxes from these sources will be discussed in another paper. A preliminary analysis of the relevant data indicates that Cassiopeia A, if observed at all, was not particularly brighter than any other object observed. Both Cygnus A and Cassiopeia A have been associated with the "secondary X-ray source" which may have been observed by Giacconi, Gursky, Paolini, and Rossi (1962). Because of the experimental results presented here, their "secondary X-ray source" may well be more appropriately identified as one or more stellar (rather than radio) sources.

V. CONCLUSIONS

1. Night-sky sources of 1–20-keV photons are not uncommon.
2. No single type of stellar object seems to be associated with the few emission regions observed.
3. As much as 10^{-3} of the total luminosity of some tentatively identified objects appears in the form of 2–8-Å photons.
4. The Crab Nebula was not the brightest X-ray source in the portion of the sky examined.
5. Detailed spectral measurements of at least some of the observed sources, in order to determine elemental abundances in the regions emitting the X-rays, probably are feasible.

We gratefully acknowledge the encouragement and assistance given to this program by J. E. Kupperian, Jr., and other personnel of NASA's Goddard Space Flight Center. Solution of the Aerobee 4.69 aspect problem by A. Boggess III, the efforts by C. Summers on both vehicle aspect problems, and the efforts in behalf of this experiment by J. R. Busse and Miss E. C. Pressly of the same facility deserve special notice. Ionospheric information was provided by Lloyd A. Lohr, of NASA, and W. W. Smith, of MIT. The flight electronics were prepared and maintained by W. Soltwedel. The assistance of H. A. Grench in the gas-flow counter development, and of D. B. Clark and K. L. Smith in the arduous task of deriving isophote flux plots, was greatly appreciated. The $\frac{1}{2}$ mil Mylar used for windows of several of the gas-flow counters was supplied by E. I. Dupont de Nemours & Co., through the courtesy of W. H. Wood. R. Helmke did much of the development work of the thin Formvar windows used on the other gas-flow counters.

Note added in proof: The calculations of Nikolsky (1963) apply to stars outside the portion of sky available to the Aerobee 4.70-detector and so do not include any of the objects included in Table 5. However, our experimental results (as expressed by conclusions 2, 3, and 5) indicate that the X-ray luminosity of some sources is larger than would be estimated by Nikolsky's computation of "quiet" radiation.

REFERENCES

- Allen, C. W. 1955, *Astrophysical Quantities* (London: Athlone Press), sec. 112.
 Babcock, H. W. 1958, *Ap. J. Suppl.*, Vol. 3, No. 30.
 Becvar, A. 1960, *Atlas Coeli II—Katalog 1950* (Cambridge: Sky Publishing Corporation).
 Edge, D. O., Shakeshaft, J. R., McAdam, W. B., Baldwin, J. R., and Archer, S. V. 1959, *Mem. R.A.S.*, 68, 37.
 Elwert, G. 1954, *Z. Naturforsch.*, 9a, 653.
 ———. 1961, *J. Geophys. Res.* 66, 391.
 Felton, J. E., and Morrison, P. 1963, *Phys. Rev. Letters*, 10, 453.
 Fisher, P. C., Meyerott, A. J., Grench, H. A., Nobles, R. A., and Reagan, J. B. 1963, *I.R.E. Transactions on Nuclear Science*, NS-10, p. 211.
 Giacconi, R., Gursky, H., Paolini, F. R., and Rossi, B. B. 1962, *Phys. Rev. Letters*, 9, 439.
 Grasberger, W., and Henyey, L. 1959, "Preliminary Report on Interplanetary X-Ray Radiation from Stellar Sources," Lawrence Radiation Laboratory, internal memorandum.
 Hoyle, F. 1963, *Ap. J.*, 137, 993.
 Hubble, E. P. 1936, *Realm of the Nebulae* (New Haven, Conn.: Yale University Press).
 Jager, C. de. 1959, *Hdb. d. Phys.*, ed. S. Flügge (Berlin: Springer-Verlag), 52, 80.
 Jenkins, L. F. 1952, *General Catalogue of Trigonometric Stellar Parallaxes* (New Haven, Conn: Yale University Observatory).
 Nikolsky, G. M. *Doklady Nauk Akad. U.S.S.R.*, 151, 536.
 Olbert, S. 1960, in *Proceedings of the Conference on X-Ray Astronomy*, held at Smithsonian Astrophysical Observatory, ed. A. E. Berman.
 Pounds, K. A., Willmore, A. P., Bowen, P. J., Norman, K., and Sanford, P. W. 1963, *Proc. Roy. Soc.*, in press.